# Analysis of Pressure Data for Fractured Wells: The Constant-Pressure Outer Boundary

R. RAGHAVAN
NICO HADINOTO
*MEMBERS SPE-AIME*

*U. OF TULSA*
*TULSA, OKLA.*

## ABSTRACT

*Analysis of flowing and shut-in pressure behavior of a fractured well in a developed five-spot fluid injection-production pattern is presented. An idealization of this situation, a fractured well located at the center of a constant-pressure square, is discussed. Both infinite-conductivity and uniform-flux fracture cases are considered. Application of log-log and semilog methods to determine formation permeability, fracture length, and average reservoir pressure is discussed.*

## INTRODUCTION

The analysis of pressure data in fractured wells has received considerable attention because of the large number of wells that have been hydraulically fractured or that intersect natural fractures. All these studies, however, were restricted to wells producing from infinite reservoirs[1,2] or to cases where the fractured well is located in a closed reservoir.[2,3] In some cases, these results were not compatible with production performance and reservoir characteristics when applied to fractured injection wells. The literature did not consider a fractured well located in a drainage area with a constant-pressure outer boundary. The most common example of such a system would be a fractured well in a developed injection-production pattern.

We studied pressure behavior (drawdown, buildup, injectivity, and falloff) for a fractured well located in a region where the outer boundaries are maintained at a constant pressure. The results apply to a fractured well in a five-spot injection-production pattern and also should be applicable to a fractured well in a water drive reservoir.[4,5] We found important differences from other systems previously reported.

We first examined drawdown behavior for a fractured well located at the center of a constant-pressure square. Both infinite-conductivity and uniform-flux solutions[1] were considered. The drawdown solutions then were used to examine buildup behavior by applying the superposition concept.[4,6] Average reservoir pressure as a function of fracture penetration ratio (ratio of drainage length to fracture length) and dimensionless time also was tabulated. This represented important new information because, as shown by Kumar and Ramey,[4] determination of average reservoir pressure for the constant-pressure outer boundary system was not as simple as that for the closed case since fluid crossed the outer boundary in an unknown quantity during both drawdown (injection) and buildup (falloff).

## MATHEMATICAL MODEL

This study employed the usual assumptions of a homogeneous, isotropic reservoir in the form of a rectangular drainage region completely filled with a slightly compressible fluid of constant viscosity. Pressure gradients were small everywhere and gravity effects were neglected. The outer boundary of the system was at constant pressure and was equal to the initial pressure of the system. The plane of the fracture was located symmetrically within the reservoir, parallel to one of the sides of the boundary (Fig. 1). The fracture extended throughout the vertical extent of the formation and fluid was produced only through the fracture at a constant rate. Both the uniform-flux and the infinite-conductivity fracture solutions were considered.[1] An infinite-conductivity fracture had no pressure drop within the fracture, whereas a

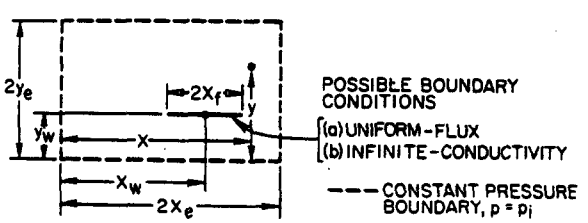


FIG. 1 — VERTICAL FRACTURE IN A RECTANGULAR RESERVOIR.

Original manuscript received in Society of Petroleum Engineers office June 1, 1976. Paper accepted for publication Jan. 14, 1977. Revised manuscript received Nov. 28, 1977. Paper (SPE 6015) was presented at the SPE-AIME 51st Annual Fall Technical Conference and Exhibition, held in New Orleans, Oct. 3-6, 1976.

This paper will be included in the 1978 *Transactions* volume.

0037-9999/78/0004-6015$00.25

uniform-flux fracture had a high, but not infinite, conductivity. Application of results to field data indicated that the uniform-flux solution was more applicable to a well intersecting a natural fracture than was the infinite-conductivity solution; however, the infinite-conductivity solution matched the behavior of hydraulically fractured wells better than the uniform-flux solution did.

This mathematical treatment assumed that the drainage boundary was rectangular and the fracture was located anywhere within the rectangle. The only other requirement for the mathematical solution was that the fracture plane be parallel to either the short or long side of the rectangle. Note that *all* the quantitative results presented here apply only to the specific case of a square drainage region with the well in the center of this square.

The mathematical solution obtained by the Greens' function product solution technique shown by Gringarten and Ramey[7] may be written as

$$p_D(x_D, y_D, t_{DA}) = 16\,(x_e/x_f)\int_0^{t_{DA}} \left\{ \sum_{n=1}^{\infty} (1/n) \cdot \exp\left[-n^2\pi^2 (y_e/x_e) t'_{DA}\right] \cdot \sin n\pi x_f/(2x_e) \sin n\pi x_w/(2x_e) \sin n\pi x/(2x_e) \right\} \left\{ \sum_{n=1}^{\infty} \exp\left[-n^2\pi^2 (x_e/y_e) \cdot t'_{DA}\right] \sin n\pi y_w/(2y_e) \cdot \sin n\pi y/(2y_e) \right\} d\,t'_{DA}, \quad \ldots\ldots\ldots\ldots\ldots\ldots\ldots\ldots\ldots\ldots (1)$$

where the dimensionless pressure drop is

$$p_D(x_D, y_D, t_{DA}) = \frac{kh}{141.2\,q\,B\mu}[p_i - p(x, y, t)], \quad \ldots\ldots\ldots\ldots\ldots\ldots\ldots\ldots\ldots\ldots (2)$$

the dimensionless time, $t_{DA}$, based on the drainage area is given by

$$t_{DA} = \frac{0.000264\,kt}{\phi\,c_t\,\mu\,A}, \quad \ldots\ldots\ldots\ldots\ldots\ldots (3)$$

dimensionless distances, $x_D$ and $y_D$, are given, respectively, by

$$x_D = \frac{x}{\sqrt{A}} \quad \text{and} \quad y_D = \frac{y}{\sqrt{A}}, \quad \ldots\ldots\ldots\ldots (4)$$

and the area is represented by

$$A = 4\,x_e\,y_e \quad \ldots\ldots\ldots\ldots\ldots\ldots\ldots (5)$$

Other symbols are shown in Fig. 1 and the bottom left corner of the rectangle is the origin.

(We caution the reader that the term drainage area used here referred to the area within the rectangle and was used mainly for convenience. In fact, the determination of drainage areas of vertically fractured wells draining a developed pattern or located in an injection-production pattern requires more in-depth study.)

Because all the quantitative results presented here pertained to a square drainage region with the well at the center, the dimensionless wellbore pressure drop was computed as follows. For the uniform-flux case the wellbore pressure drop, $p_{wD}$, was computed at $x_D = y_D = 0.5$. For the infinite-conductivity case it was not readily apparent how Eq. 1 could be used to calculate the pressure drop. It was shown in Ref. 1 that the uniform-flux solution could be used to obtain an approximate infinite-conductivity unsteady-state solution (that is, satisfying the boundary conditions exactly after a certain period of time) by computing the pressure drop at $x_D = 0.5 + 0.732\,x_{fD}$, $y_D = 0.5$, where $x_{fD} = x_f/\sqrt{A}$. Gringarten *et al.* obtained this result by breaking up the fracture length into discrete elements and adjusting the withdrawal from each element by trial and error until the pressure at any given time over the entire fracture length was uniform to as high an accuracy as desired. They then showed that the infinite-conductivity wellbore pressure drop could be obtained to within 0.1-percent accuracy by assuming a uniform-flux distribution and computing the pressure drop at $x_D = 0.5 + 0.732\,x_{fD}$, $y_D = 0.5$. Results obtained by finite-difference techniques also have shown that this approach is valid. For very early times, the uniform-flux and infinite-conductivity solutions are identical.[1] In all the results shown here $x_{wD} = y_{wD} = 0.5$.

For small values of dimensionless time it can be shown that, for all points on the fracture plane,

$$p_D(x_D, 0.5, t_{Dx_f}) = \sqrt{\pi\,t_{Dx_f}}, \quad \ldots\ldots\ldots (6)$$

where $t_{Dx_f}$ is the dimensionless time based on the fracture half length, $x_f$, and is given by

$$t_{Dx_f} = t_{DA}\,\frac{A}{x_f^2} \quad \ldots\ldots\ldots\ldots\ldots (7)$$

$$= t_{DA}\,\frac{(2x_e)^2}{x_e^2} = 4\left(\frac{y_e}{x_e}\right)(t_{DA})$$

## TRANSIENT FLOW INFORMATION

Figs. 2 and 3 are log-log graphs that present the dimensionless wellbore pressure drop, $p_{wD}$, vs dimensionless time, $t_{Dx_f}$, obtained by integrating Eq. 1 for the infinite-conductivity and uniform-flux cases, respectively (see also Tables 1 and 2). In both figures, solutions for the dimensionless pressure drop at a fractured well located at the center of a closed square are given for comparison. The $x_e/x_f = \infty$ line in Figs. 2 and 3 represents a vertically fractured well in an infinite reservoir and not an *unfractured well*. A detailed treatment of the flow behavior of a vertically fractured well in an infinite reservoir may be found in Ref. 1.

The results in Figs. 2 and 3 indicate three characteristic flow periods. A linear flow period occurs at early times when the fracture controls flow behavior. This period is characterized by a straight line of slope equal to 0.5 on log-log

TABLE 1 — DIMENSIONLESS WELLBORE PRESSURE DROP FOR AN INFINITE-CONDUCTIVITY VERTICAL FRACTURE AT THE CENTER OF A CONSTANT-PRESSURE SQUARE

$t_{DA(x_f)} = 4\left(\frac{x_e}{x_f}\right)^2 (t_{DA})$

| Dimensionless Time, $t_{DA}$ — Fracture Penetration Ratio, $x_e/x_f$ | Dimensionless Wellbore Pressure Drop, $p_{wD}$* | | | | | | | |
|---|---|---|---|---|---|---|---|---|
| | 1 | 1.5 | 2 | 3 | 5 | 7 | 10 | 15 |
| 0.00200 | 0.15784 | | | | | | | |
| 0.00300 | 0.19142 | | | | | | | |
| 0.00400 | 0.21820 | | | | | | | |
| 0.00500 | 0.24050 | | | | | | | |
| 0.00600 | 0.25962 | | | | | | | |
| 0.00700 | 0.27635 | 0.40797 | | | | | | |
| 0.00800 | 0.29123 | 0.43153 | | | | | | |
| 0.00900 | 0.30462 | 0.45325 | | | | | | |
| 0.01000 | 0.31679 | 0.47346 | | | | | | |
| 0.01500 | 0.36368 | 0.54979 | 0.69375 | 0.94886 | 1.31317 | 1.65473 | 1.99999 | 2.38611 |
| 0.02000 | 0.40058 | 0.62611 | 0.78873 | 1.07177 | 1.50330 | 1.81527 | 2.15836 | 2.55643 |
| 0.03000 | 0.45173 | 0.73127 | 0.92096 | 1.23463 | 1.68940 | 2.00912 | 2.35661 | 2.75712 |
| 0.04000 | 0.48851 | 0.81138 | 1.02216 | 1.35602 | 1.82405 | 2.14790 | 2.49769 | 2.89946 |
| 0.05000 | 0.51689 | 0.87491 | 1.10259 | 1.45129 | 1.92829 | 2.25483 | 2.60608 | 3.00864 |
| 0.06000 | 0.53954 | 0.92623 | 1.16763 | 1.52790 | 2.01157 | 2.34006 | 2.69237 | 3.09550 |
| 0.07000 | 0.55790 | 0.96805 | 1.22066 | 1.59019 | 2.07910 | 2.40909 | 2.76222 | 3.16579 |
| 0.08000 | 0.57287 | 1.00227 | 1.26405 | 1.64110 | 2.13421 | 2.46542 | 2.81919 | 3.22310 |
| 0.09000 | 0.58513 | 1.03031 | 1.29962 | 1.68281 | 2.17934 | 2.51152 | 2.86582 | 3.27002 |
| 0.10000 | 0.59518 | 1.05332 | 1.32880 | 1.71702 | 2.21634 | 2.54932 | 2.90405 | 3.30847 |
| 0.20000 | 0.63481 | 1.14405 | 1.44388 | 1.85192 | 2.36223 | 2.69834 | 3.05475 | 3.46008 |
| 0.30000 | 0.64031 | 1.15665 | 1.45987 | 1.87066 | 2.38249 | 2.71903 | 3.07568 | 3.48113 |
| 0.40000 | 0.64108 | 1.15840 | 1.46209 | 1.87326 | 2.38531 | 2.72191 | 3.07859 | 3.48406 |
| 0.50000 | 0.64118 | 1.15865 | 1.46240 | 1.87362 | 2.38570 | 2.72231 | 3.07899 | 3.48446 |
| > 0.60000 | 0.64120 | 1.15868 | 1.46244 | 1.87368 | 2.38575 | 2.72236 | 3.07905 | 3.48452 |

*Values of $p_{wD}$ for times smaller than that shown here are identical to the closed outer boundary case.

coordinates and is commonly referred to as the one-half slope line. After a transition period, a pseudo-radial flow period exists. Data in the pseudo-radial flow period have a characteristic slope of 1.151/log~ on semilog coordinates. This period, however, exists for only certain values of $x_e/x_f$. For the uniform-flux case, this period is absent for fracture penetration ratios less than 3 and for infinite-conductivity fractures for $x_e/x_f$ less than 5. After a second transition period, steady-state flow occurs for all $x_e/x_f$ similar to that of an unfractured well in a constant-pressure square. This period is analogous to pseudo-steady-state flow behavior for wells in closed systems. During steady state the pressure at each point in the system is time invariant. The system reaches steady state at a $t_{DA}$ of about 0.4 for all $x_e/x_f$.

For practical purposes, Figs. 2 and 3 may be used for type-curve matching for the appropriate fracture type.[2] If a drainage limit became evident during the test, then data points would follow the appropriate $x_e/x_f$ line. If the system under study is located in a constant-pressure square, then field data would fall below the $x_e/x_f = \infty$ curve and follow the appropriate $x_e/x_f$ line. On the other hand, if the system boundaries are closed, then data would rise above the $x_e/x_f = \infty$ curve and follow the corresponding $x_e/x_f$ line. Figs. 2 and 3 also may be used for analyzing falloff or buildup data.[1,2] This aspect of pressure analysis will be considered in the section on shut-in pressure behavior.

For unfractured wells, Hurst *et al.*[8] remarked that the time at which system boundaries (closed or constant-pressure) affect pressure behavior is the same; that is, curves influenced by outer boundary

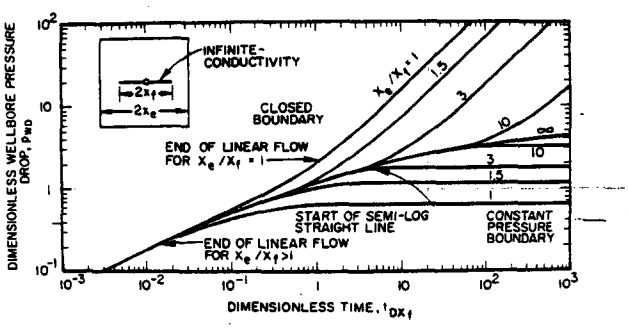


FIG. 2 — DIMENSIONLESS WELLBORE PRESSURE DROP VS DIMENSIONLESS TIME FOR AN INFINITE-CONDUCTIVITY VERTICAL FRACTURE.

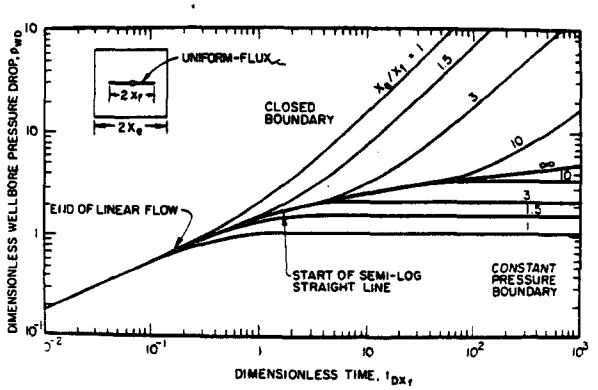


FIG. 3 — DIMENSIONLESS WELLBORE PRESSURE DROP VS DIMENSIONLESS TIME FOR A UNIFORM-FLUX VERTICAL FRACTURE.

conditions will depart simultaneously from the infinite reservoir curve, regardless of the nature of the outer boundary. The results in Figs. 2 and 3 indicate that for practical purposes this observation also holds for all cases except $x_e/x_f = 1$. This implies that a limiting statement can be made concerning the drainage volume for a fractured well that does not indicate a drainage boundary effect for both closed and constant-pressure boundary cases provided $x_e/x_f \neq 1$; that is, if the fracture does not extend to the outer boundary.

Comparison of Figs. 2 and 3 for the closed and constant-pressure cases for $x_e/x_f = 1$ indicates one important difference. The pressure drops are identical for the uniform-flux and infinite-conductivity cases for the closed reservoir, whereas for the constant-pressure case this is not so. These results are caused by the influence of the outer boundary. If $x_e/x_f = 1$, no pressure gradients parallel to the fracture plane exist in a closed reservoir; in the constant-pressure case this is not so.

## AVERAGE RESERVOIR PRESSURE

In the case of a closed reservoir, the average reservoir pressure in an area drained by a well may be obtained from a simple materials balance. For a well in a closed system producing at a constant rate, the dimensionless average pressure obtained by a materials balance is given by

$$\bar{p}_D(t_{DA}) = \frac{kh}{141.2\,qB\mu}[p_i - \bar{p}(t)] = 2\pi t_{DA} \cdot \quad \ldots\ldots\ldots\ldots\ldots\ldots\ldots\ldots\ldots\ldots (8)$$

For the system under study here, the average reservoir pressure cannot be obtained readily from a materials balance unless the quantity of fluid crossing the constant pressure boundary is known. Dimensionless average reservoir pressures may be calculated, however, by integrating Eq. 1 over the drainage area. These are shown in Table 3 and are accurate to five digits.

The $\bar{p}_D(t_{DA})$ values presented in Table 3 represent important new information. Theoretically, if a well producing from a *bounded* system is shut in, then the wellbore pressure will stabilize at the mean pressure of the area drained at the instant the well is shut in. However, in the system examined here the final pressure will not stabilize at the mean pressure of the system but at the pressure corresponding to that of the outer boundary, namely $p_i$. Furthermore, the average reservoir pressure during buildup changes as fluid crosses the reservoir boundary. In most engineering applications such as material-balance computations, the average reservoir pressure at the *instant* of shut-in and not at the *end* of the buildup period is required. Once $p_i$ is determined, the information shown in Table 3 can be used to calculate the average reservoir pressure. This will be examined further in considering aspects of buildup.

At this point, one qualifying remark about Table 3 is necessary. Strictly speaking, the results presented by Table 3 are rigorously correct only for the uniform-flux case. As pointed out by Gringarten *et al.*[1], the flux distribution per unit area of the fracture for the infinite-conductivity fracture changes with time until the flux distribution reaches a stablized condition at long times (Fig. 2 of Ref. 1). This distribution is different from the uniform-flux case and thus the areal pressure distribution around the fracture would be different. To our knowledge, no *simple method* exists for determining pressure distribution surrounding an infinite-conductivity vertical fracture, although the pressure at the fracture may be readily determined using the procedure of Gringarten *et al.* Thus, the results in Table 3 should be understood to be somewhat approximate, especially when applying

$t_{D(x_f)} = (t_{DA}) \times (4)\left(\frac{x_e}{x_f}\right)^2$

TABLE 2 — DIMENSIONLESS WELLBORE PRESSURE DROP FOR A UNIFORM-FLUX VERTICAL FRACTURE AT THE CENTER OF A CONSTANT-PRESSURE SQUARE

| Dimensionless Time, $t_{DA}$ — Fracture Penetration Ratio, $x_e/x_f$ | Dimensionless Wellbore Pressure Drop, $p_{wD}$* | | | | | | | |
|---|---|---|---|---|---|---|---|---|
| | 1 | 1.5 | 2 | 3 | 5 | 7 | 10 | 15 |
| 0.01000 | 0.35447 | 0.53060 | | | | | | |
| 0.02000 | 0.50001 | 0.73915 | | | | | | |
| 0.03000 | 0.60695 | 0.88494 | 1.11788 | | | | | |
| 0.04000 | 0.69069 | 0.99613 | 1.24159 | 1.61427 | 2.10733 | | | |
| 0.05000 | 0.75790 | 1.08433 | 1.33856 | 1.71813 | 2.21496 | 2.54761 | 2.90216 | |
| 0.06000 | 0.81250 | 1.15558 | 1.41647 | 1.80114 | 2.30071 | 2.63412 | 2.98909 | 3.40543 |
| 0.07000 | 0.85711 | 1.21364 | 1.47981 | 1.86846 | 2.37013 | 2.70414 | 3.05942 | 3.47593 |
| 0.08000 | 0.89364 | 1.26114 | 1.53157 | 1.92341 | 2.42677 | 2.76125 | 3.11678 | 3.53343 |
| 0.09000 | 0.92360 | 1.30007 | 1.57398 | 1.96841 | 2.47313 | 2.80799 | 3.16372 | 3.58048 |
| 0.10000 | 0.94818 | 1.33201 | 1.60875 | 2.00530 | 2.51113 | 2.84630 | 3.20220 | 3.61905 |
| 0.20000 | 1.04514 | 1.45798 | 1.74589 | 2.15076 | 2.66097 | 2.99736 | 3.35391 | 3.77122 |
| 0.30000 | 1.05861 | 1.47547 | 1.76494 | 2.17096 | 2.68178 | 3.01834 | 3.37498 | 3.79236 |
| 0.40000 | 1.06048 | 1.47790 | 1.76758 | 2.17377 | 2.68467 | 3.02125 | 3.37790 | 3.79529 |
| 0.50000 | 1.06074 | 1.47824 | 1.76795 | 2.17416 | 2.68507 | 3.02166 | 3.37831 | 3.79576 |
| 0.60000 | 1.06078 | 1.47829 | 1.76800 | 2.17421 | 2.68513 | 3.02171 | 3.37837 | 3.79576 |
| > 0.70000 | 1.06079 | 1.47829 | 1.76801 | 2.17422 | 2.68514 | 3.02172 | 3.37837 | 3.79576 |

*Values of $p_{wD}$ for times smaller than that shown here are identical to the closed outer boundary case.

them to actual field problems for infinite-conductivity fractures.

## THE EFFECTIVE WELLBORE RADIUS

Many authors have interpreted the behavior of a a fractured well in terms of an equivalent unfractured system using the concept of an effective wellbore radius. Prats[9] has shown that steady-state production of an incompressible fluid via an infinite-conductivity vertical fracture from a closed circular reservoir may be described by an unfractured well with an effective radius equal to one-half of the fracture half-length, for ratios of reservoir radius to fracture half-length greater than 2. This also holds for the flow of a compressible fluid at *pseudo steady state*.[10] The effective wellbore radius at steady state for an infinite-conductivity or uniform-flux vertical fracture for the present case can be obtained from

$$p_{wD}\,(t_{DA}) = \ln\left[\frac{8\,(x_f/r_w')}{\sqrt{\exp(\gamma)\,C_A}}\,\frac{x_e}{x_f}\right], \quad \ldots\ldots (9)$$

where $C_A$ is the shape factor for a well in a closed square and $r_w'$ is the effective wellbore radius. Effective radii computed from Eq. 9 and corresponding results for the closed outer boundary case are shown in Fig. 4. It is evident from these results that the nature of the outer boundary must be taken into account if this concept is to be used to describe pressure behavior at the well.

Clarification of the value for the shape factor used in Eq. 9 is needed here. Kumar and Ramey[4] have shown that the value for $C_A$ depends on whether the defining equation for the shape factor involves $(p_i - p_{wf})$ or $(\bar{p} - p_{wf})$. As they pointed out, the equation involving $(p_i - p_{wf})$ is a more fundamental definition. If $(p_i - p_{wf})$ is used for defining the shape factor, then $C_A = 30.88$ regardless of whether the outer boundary conditions are closed or at constant pressure. [However, we do not know if this observation applies for other drainage shapes even if $(p_i - p_{wf})$ is used.]

## SHUT-IN PRESSURE BEHAVIOR

Buildup pressures at the fractured well may be analyzed along conventional lines using the radial-flow idealization[11-13] at late times and the linear-flow approximation[14] at early times. More

TABLE 3 — DIMENSIONLESS AVERAGE PRESSURE DROP, $\bar{p}_D$, VS DIMENSIONLESS TIME, $t_{DA}$, FOR A VERTICAL FRACTURE LOCATED AT THE CENTER OF A CONSTANT-PRESSURE SQUARE

| Dimensionless Time, $t_{DA}$ — Fracture Penetration Ratio, $x_e/x_f$ | Dimensionless Average Pressure Drop, $\bar{p}_D$* | | | | | | | |
|---|---|---|---|---|---|---|---|---|
| | 1 | 1.5 | 2 | 3 | 5 | 7 | 10 | 15 |
| 0.0002 | 0.00124 | | | | | | | |
| 0.0003 | 0.00185 | | | | | | | |
| 0.0004 | 0.00245 | | | | | | | |
| 0.0005 | 0.00305 | | | | | | | |
| 0.0006 | 0.00364 | | | | | | | |
| 0.0007 | 0.00423 | | | | | | | |
| 0.0008 | 0.00482 | | | | | | | |
| 0.0009 | 0.00541 | | | | | | | |
| 0.0010 | 0.00599 | | | | | | | |
| 0.0020 | 0.01173 | 0.01257 | 0.01257 | 0.01257 | 0.01257 | 0.01257 | 0.01257 | 0.01257 |
| 0.0030 | 0.01731 | 0.01884 | 0.01885 | 0.01885 | 0.01885 | 0.01885 | 0.01885 | 0.01885 |
| 0.0040 | 0.02275 | 0.02510 | 0.02513 | 0.02513 | 0.02513 | 0.02513 | 0.02513 | 0.02513 |
| 0.0050 | 0.02808 | 0.03132 | 0.03141 | 0.03142 | 0.03142 | 0.03142 | 0.03142 | 0.03142 |
| 0.0060 | 0.03332 | 0.03751 | 0.03768 | 0.03770 | 0.03770 | 0.03770 | 0.03770 | 0.03770 |
| 0.0070 | 0.03846 | 0.04366 | 0.04393 | 0.04398 | 0.04398 | 0.04398 | 0.04398 | 0.04398 |
| 0.0080 | 0.04351 | 0.04975 | 0.05017 | 0.05025 | 0.05026 | 0.05026 | 0.05026 | 0.05026 |
| 0.0090 | 0.04849 | 0.05580 | 0.05638 | 0.05651 | 0.05654 | 0.05654 | 0.05654 | 0.05654 |
| 0.0100 | 0.05338 | 0.06179 | 0.06256 | 0.06277 | 0.06281 | 0.06281 | 0.06282 | 0.06282 |
| 0.0200 | 0.09851 | 0.11826 | 0.12187 | 0.12357 | 0.12419 | 0.12433 | 0.12440 | 0.12444 |
| 0.0300 | 0.13689 | 0.16731 | 0.17443 | 0.17842 | 0.18013 | 0.18056 | 0.18078 | 0.18090 |
| 0.0400 | 0.16896 | 0.20868 | 0.21913 | 0.22549 | 0.22839 | 0.22915 | 0.22954 | 0.22975 |
| 0.0500 | 0.19550 | 0.24304 | 0.25641 | 0.26491 | 0.26891 | 0.26997 | 0.27053 | 0.27082 |
| 0.0600 | 0.21737 | 0.27140 | 0.28724 | 0.29756 | 0.30251 | 0.30384 | 0.30453 | 0.30491 |
| 0.0700 | 0.23535 | 0.29474 | 0.31264 | 0.32447 | 0.33022 | 0.33177 | 0.33259 | 0.33302 |
| 0.0800 | 0.25012 | 0.31392 | 0.33351 | 0.34661 | 0.35302 | 0.35475 | 0.35566 | 0.35615 |
| 0.0900 | 0.26225 | 0.32967 | 0.35066 | 0.36479 | 0.37175 | 0.37363 | 0.37462 | 0.37515 |
| 0.1000 | 0.27221 | 0.34261 | 0.36474 | 0.37972 | 0.38713 | 0.38914 | 0.39020 | 0.39076 |
| 0.2000 | 0.31150 | 0.39365 | 0.42031 | 0.43866 | 0.44784 | 0.45034 | 0.45166 | 0.45237 |
| 0.3000 | 0.31696 | 0.40074 | 0.42803 | 0.44685 | 0.45627 | 0.45884 | 0.46020 | 0.46093 |
| 0.4000 | 0.31772 | 0.40173 | 0.42910 | 0.44799 | 0.45744 | 0.46002 | 0.46139 | 0.46212 |
| 0.5000 | 0.31782 | 0.40186 | 0.42925 | 0.44815 | 0.45761 | 0.46019 | 0.46155 | 0.46228 |
| ≥ 0.6000 | 0.31784 | 0.40188 | 0.42927 | 0.44817 | 0.45763 | 0.46021 | 0.46158 | 0.46231 |

*For times earlier than those shown here the following equation applies.

$$\bar{p}_D = \frac{kh}{141.2\,qB\mu}\left[p_i - \bar{p}\,(t)\right] = 2\pi t_{DA}\,.$$

recently, type-curve matching has been proposed to analyze pressure data.[1,2]

Application of the type-curve and linear-flow approximation procedures to the problem under consideration is similar to that discussed in Refs. 2 and 14 and so will not be discussed in detail here. Although these procedures are well known, one point should be emphasized regarding application of log-log type curves in Figs. 2 and 3 to pressure buildup or falloff data by the type-curve matching procedure. On a log-log graph, the ordinate must be the absolute difference between the flowing pressure at the start of the test and the shut-in pressure during the test vs the logarithm of the shut-in time. This is based directly on the work of Agarwal *et al.*[15]

The results for the semilog graphs are different from previous studies. Determination of the permeability-thickness product by the conventional semilog approach requires significant corrections. In general, determination of permeability by this method is a trial-and-error process because the fracture length also influences the slope of the straight line. Thus, the log-log approach is preferable for estimating the permeability-thickness product and fracture length. However, the semilog methods, particularly the Miller-Dyes-Hutchinson method,[12] are advantageous for calculating the average reservoir pressure.

## SEMILOG BUILDUP GRAPHS

We shall now examine common methods of buildup analysis as they apply to a fractured well in a constant-pressure square. The basic equation required to generate buildup data is

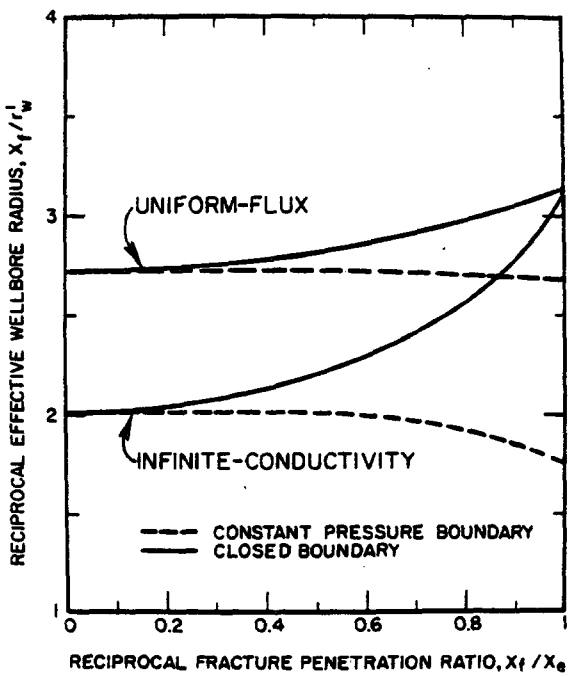


FIG. 4 — RECIPROCAL DIMENSIONLESS EFFECTIVE WELLBORE RADIUS VS RECIPROCAL FRACTURE PENETRATION RATIO.

$$p_{Ds} = \frac{kh}{141.2\,qB\mu}(p_i - p_{ws})$$
$$= p_{wD}[x_e/x_f, (t + \Delta t)_{DA}]$$
$$- p_{wD}(x_e/x_f, \Delta t_{DA}) \ldots\ldots\ldots (10)$$

The conventional approach to the analysis of shut-in pressures has been to replace the right side of Eq. 10 with appropriate analytical expressions, to plot buildup data accordingly, and then to examine them for significant characteristics. However, recent studies[5,6] have indicated that previous assumptions, although sufficient, were unnecessary and that general empirical methods may be used to examine shut-in pressure behavior. We have adopted this approach here in examining the basic characteristics of the common semilog buildup plots (Muskat,[11] Miller-Dyes-Hutchinson, and Horner[13]). Because the application of these methods to fractured wells was reviewed recently, only the essential differences between this study and that of Raghavan *et al.*[16] will be considered. From a discussion of the drawdown solutions it should be evident that buildup graphs for both uniform-flux and infinite-conductivity fractures are required. Only the infinite-conductivity case will be examined in detail.

### THE EXTENDED MUSKAT METHOD

The extended Muskat method involved a plot of the logarithm of $(\bar{p} - p_{ws})$ vs shut-in time for closed bounded systems. For the constant-pressure outer boundary case, however, a more appropriate pressure difference was $(p_i - p_{ws})$.[4] Eq. 10 is the basis for obtaining generalized Muskat graphs. The objective of this method was to find a straight line when the correct value of $p_i$ has been selected by trial. The slope of the correct Muskat straight line was proportional to the hydraulic diffusivity, and the intercept of this straight line was proportional to the permeability-thickness product.[4-6]

Fig. 5 is a typical Muskat graph for $x_e/x_f = 15$ and for a range of producing times up to steady state. It shows straight lines did form for the correct value of $p_i$ and all were parallel for the producing times considered. Because the slope of the correct Muskat straight line is proportional to the hydraulic diffusivity, the correct diffusivity or the porosity-compressibility product can be obtained from this graph. Similar results were also obtained for other values of $x_e/x_f$. The permeability-thickness product may be obtained by extrapolating the correct straight line and determining the intercept. The intercepts of the various straight lines are a strong function of producing time. Thus, the effect of producing time must be taken into account in determining the permeability-thickness product, $kh$, by this method.

Fig. 6 provides the information required to determine the $kh$ product by this method as a function of $x_f/x_e$ and producing time. The $kh$ product may be determined from the following equation.

$$kh = \frac{141.2\, qB\, \mu}{(p_i - p_{ws})_{\Delta t=0}} [b\,(x_f/x_e, t_{DA})] , \quad . \quad .(11)$$

where $b$ is the ordinate given in Fig. 6. The denominator was obtained by extrapolating the correct straight line of the field data to zero shut-in time.

In Fig. 6 we used $x_f/x_e$ so it would be possible to compare results with an unfractured well in a constant-pressure square as well as with those results presented in Ref. 16 ($x_f/x_e = 0$ corresponds to an *unfractured* well in a constant-pressure square).

The porosity-compressibility product may be obtained from the slope of the Muskat graph, as mentioned. Examination of the Muskat graph for various penetration ratios indicated the slopes were not a function of $x_e/x_f$. The slopes of the correct straight lines were approximately constant and equal to $0.1111^{-1}$ log ~. Thus, the $\phi c_t$ product may be calculated by

$$\phi c_t = -0.0571 \frac{k}{\mu A m} , \quad . \quad . \quad . \quad . \quad . \quad . \quad . \quad . \quad . \quad (12)$$

where $m$ is the slope of the correct Muskat straight line in log ~/D. Here the symbol "log" refers to "logarithm to the base 10."

A comparison of these results with corresponding cases for a vertically fractured well in a closed square indicated that the intercepts presented here were about the same (for small $x_e/x_f$) or larger (for large $x_e/x_f$) than those reported in Ref. 16. On the other hand, values of the slopes obtained here were much smaller than those given in Ref. 16. The higher intercept and lower slope values resulted from the increase in the general pressure level because of the presence of the constant-pressure boundary.

Two other aspects of the Muskat graph also deserve attention. These pertain to the duration of time for which the Muskat straight line exists. All curves in Fig. 5 straightened out only after a minimum shut-in time shown by the left-hand dashed line. This minimum time increased as the producing time decreased, and it also was dependent on $x_e/x_f$. Fig. 7 presents the shut-in times required for the start of the Muskat straight line as a function of $x_e/x_f$ and $t_{DA}$. As the flowing time approached steady state, the value of the shut-in time needed to reach the proper straight line became independent

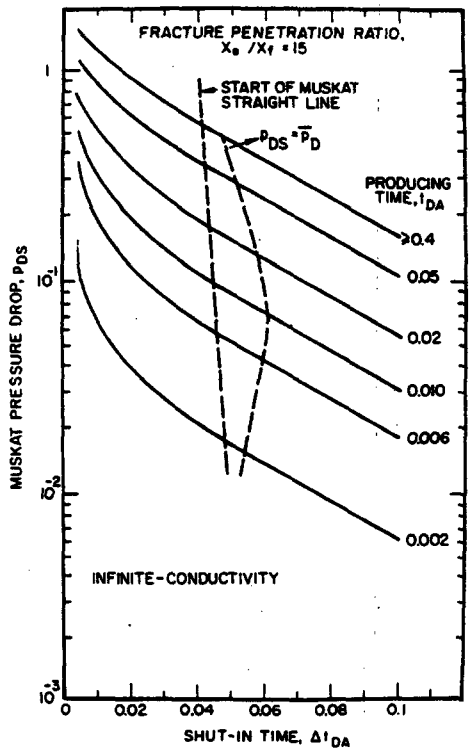


FIG. 5 — MUSKAT GRAPH FOR A VERTICALLY FRACTURED WELL IN A CONSTANT-PRESSURE SQUARE.

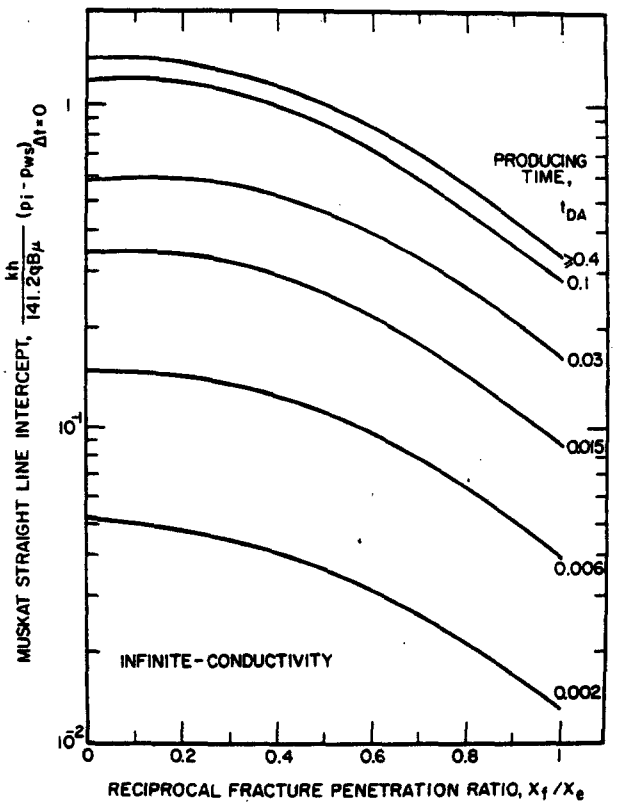


FIG. 6 — MUSKAT GRAPH INTERCEPT VS PRODUCING TIME FOR A VERTICALLY FRACTURED WELL IN A CONSTANT-PRESSURE SQUARE.

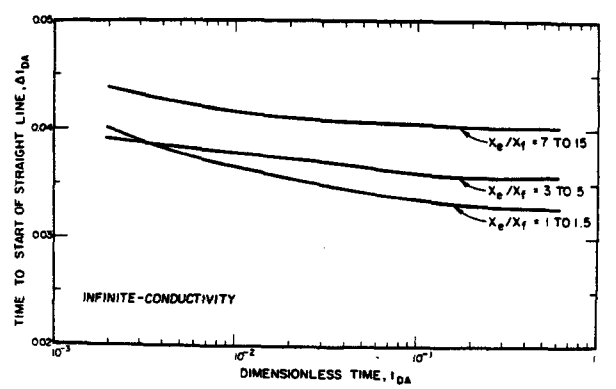


FIG. 7 — BUILDUP TIME TO START OF MUSKAT STRAIGHT LINE FOR A VERTICALLY FRACTURED WELL IN A CONSTANT-PRESSURE SQUARE.

of the flowing time.

As a result of the above requirement, a thorough analysis of pressure data by the Muskat method required that dimensionless time checks be made with the help of Fig. 7 to assure that the test had been run long enough and the proper straight line was chosen. This lower limit was important because apparent straight lines *could* be obtained on the Muskat graph for times less than those shown in Fig. 7, yielding an incorrect low value of initial pressure, $p_i$.

As studies have shown,[4-6,16] an upper limit also existed for the duration of the straight line, because, in general, data beyond that required to reach steady state could not be analyzed by the Muskat method. This implied an upper time limit of $\Delta t_{DA} = 0.4$.

It should be clear from the above discussion that unlike the closed drainage area, the average reservoir pressure in the area drained at the instant of shut-in could not be directly obtained by the Muskat method. The procedure would be to first determine $p_i$ and then estimate the average reservoir pressure from Table 3. The right-hand dashed line in Fig. 5 shows the shut-in times at which $p_{ws} = \bar{p}$.

## THE MILLER-DYES-HUTCHINSON METHOD

The Miller-Dyes-Hutchinson (MDH) method required that buildup pressures be plotted as a function of the logarithm of shut-in time. A dimensionless MDH buildup graph was first presented by Perrine.[17] As in the case of the Muskat graph, Eq. 10 was the basis for preparing the dimensionless MDH graph. We followed the general procedure outlined by Ramey and Cobb[6] and examined this method for a wide range of producing times rather than taking the classical approach of assuming long producing time prior to shut-in. Fig. 8 is a typical MDH graph obtained in this study.

In a conventional MDH graph for an unfractured well, a linear portion with a slope of 1.151/log ~

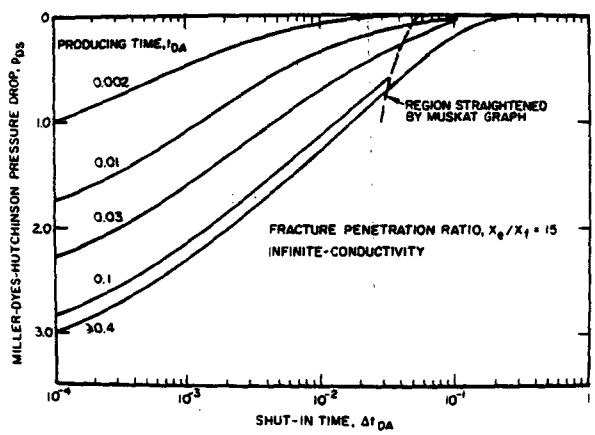


FIG. 8 — MILLER-DYES-HUTCHINSON BUILDUP GRAPH FOR VERTICALLY FRACTURED WELL IN A CONSTANT-PRESSURE SQUARE (INFINITE-CONDUCTIVITY).

was evident for early shut-in times. However, in Fig. 8, no well defined straight line was evident. The maximum slope for any of the curves on Fig. 8 was 0.965, much less than the expected value of 1.151. In addition, the maximum slope decreased as producing time decreased. This type of behavior was typical of this method of analysis for a vertically fractured well. Raghavan *et al.*[16] described a similar effect for closed drainage systems. They noted that the reduced slope would lead an analyst to compute large permeability-thickness values and thus ascribe this result to the opening of "new sand" after fracturing. Though this could happen, the results shown in Fig. 8 indicated that the slope of the apparent MDH straight line for a fractured well was much less than that for an unfractured well.

The curve in Fig. 8 for producing times $t_{DA} \geq 0.4$ represented steady-state behavior before shut-in. As in the unfractured well case, a single curve resulted for this condition. Fig. 8 also shows the region of the buildup data straightened by the Muskat graph.

At this stage, an apparent paradox regarding this type of a graph should be clarified. Earlier discussions on drawdown pointed out that a pseudo-radial flow period existed. Thus, one should have expected a slope of 1.151/log cycle at least for this penetration ratio. This slope was not obtained for two reasons. First, for small values of producing time the proper MDH straight line lasted very briefly.[6] During the corresponding period for this instance, linear rather than radial flow prevailed. The second reason for this result was the superposition principle in Eq. 10 for obtaining the buildup curves.

Fig. 8 raises serious questions about the applicability of this type of graph for determining formation flow capacity. A method was proposed[16] for correcting the slopes of the apparent straight line for the case of a fractured well in a closed square. It was suggested that the maximum slope be read for the fractured well buildup and then the permeability be corrected to the true value. Fig. 9 presents permeability-thickness correction factors for the MDH method of graphical analysis as a family of dashed lines for a fractured well in a constant-pressure square. The correction factors were obtained from plots similar to Fig. 8 by dividing the maximum slope by 1.151. The solid lines represent similar correction factors for the Horner graph and will be discussed later. As shown in Fig. 9, in most instances the correction factors for the MDH graph were considerably less than those for the Horner graph. This implied that the apparent permeability-thickness from this procedure could be in greater error than that obtained by the Horner method. A step-by-step procedure to estimate the permeability-thickness product, $kh$, by this approach is given in Ref. 16.

The above discussion indicates a log-log type-curve analysis should be more reliable than the MDH method for estimating formation flow

capacity because one must be *certain* the test was run *long enough* to obtain the *maximum slope*. The fracture penetration ratio had to be known to use the correction factors shown in Fig. 9, whereas in the type-curve procedure this was not the case. All the field data examined confirmed this observation.

Although the MDH procedure is not recommended for determining $kh$, graphs such as those in Fig. 8 are useful for determining average reservoir pressure, $\bar{p}$. The following procedure is recommended to calculate average reservoir pressure by this method.

1. Dimensionless flowing time, $t_{DA}$, and dimensionless shut-in time, $\Delta t_{DA}$, are calculated corresponding to *any* value of shut-in time, $\Delta t$.

2. For the appropriate value of fracture penetration ratio, $x_e/x_f$, and dimensionless time, $\Delta t_{DA}$, calculated in Step 1, a dimensionless pressure drop is read from a graph such as Fig. 8.

3. The pressure at the outer boundary is calculated by

$$p_i = p_{ws} + \frac{141.2\, qB\mu}{kh}\, p_{Ds}\,, \quad \ldots\ldots\ldots \quad (13)$$

where $p_{ws}$ is the shut-in pressure corresponding to the time used in determining $\Delta t_{DA}$ in Step 1.

4. The average reservoir pressure may be obtained for the appropriate dimensionless producing time and fracture penetration ratio by the expression

$$\bar{p} = p_i - \frac{141.2\, qB\mu}{kh}\, \bar{p}_D\,, \quad \ldots\ldots\ldots \quad (14)$$

where $\bar{p}_D$ may be obtained from Table 3.

This recommendation to determine average pressure differs from that in Refs. 3 and 16. Those authors recommended use of the Muskat graph, but considering the portion of the buildup data straightened by that graph (Fig. 8), in practice it would be unusual for the test to be run for that period of time. The Muskat method would be more useful if the test were run for a long enough period.

## THE HORNER METHOD

The Horner method required a graph of the shut-in pressures, $p_{ws}$, vs the logarithm of $(t + \Delta t)/\Delta t$. Here, $t$ was the producing time before shut-in and $\Delta t$ was the shut-in time. Eq. 10 also was used in this instance to obtain synthetic Horner graphs.

Fig. 10 presents the Horner graph for a vertically fractured well located in a constant-pressure square. There is an important difference between the graph shown here and the Horner graph for the closed square. Unlike the closed case, the shut-in wellbore pressure reached $p_i$ for all producing times because of fluid recharge across the constant-pressure boundary. As in the MDH graph, no extensive linear portion was evident. Fig. 10, however, indicates that all curves approached a common value of maximum slope for $t_{DA} \leq 0.1$. For larger values of $t_{DA}$ the maximum slope increased. The synthetic Horner graphs for values of $x_e/x_f$ examined in this study indicated that the change in maximum slope occurred only if $x_e/x_f \geq 1.5$.

Permeability-thickness correction factors were also prepared for the Horner graph. The results are shown as two solid lines in Fig. 9; as mentioned, the maximum slope changed after a certain value of producing time for $x_e/x_f \geq 1.5$, requiring two lines.

A comparison of the shape of the buildup curves shown in Fig. 10 with that of an unfractured well in a constant-pressure square also showed an important difference. Kumar and Ramey showed that as producing time increased, the curves moved to the right and suggested that a system under recharge could be identified by this property. In this instance, however, the curves moved to the left for brief producing times before moving back to the right. Thus, the suggestion to identify a constant-pressure boundary system by pressure buildup or

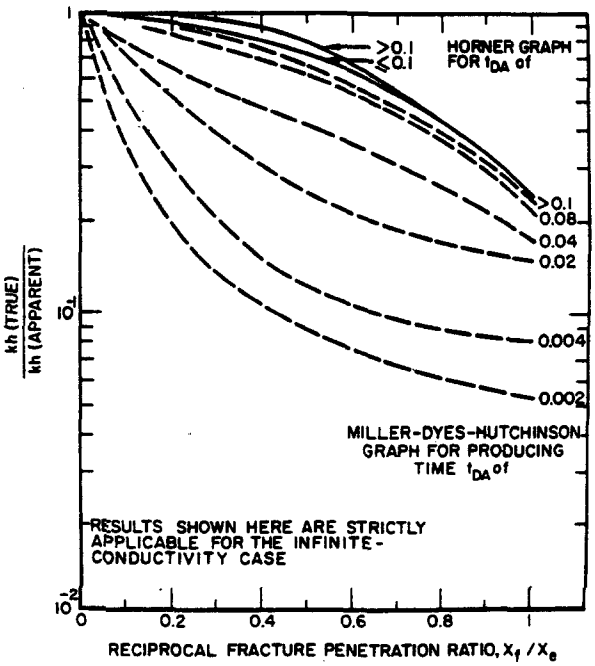


FIG. 9 — $kh$ FACTOR VS FRACTURE PENETRATION RATIO FOR MILLER-DYES-HUTCHINSON AND HORNER BUILDUP GRAPHS (CONSTANT-PRESSURE SQUARE).

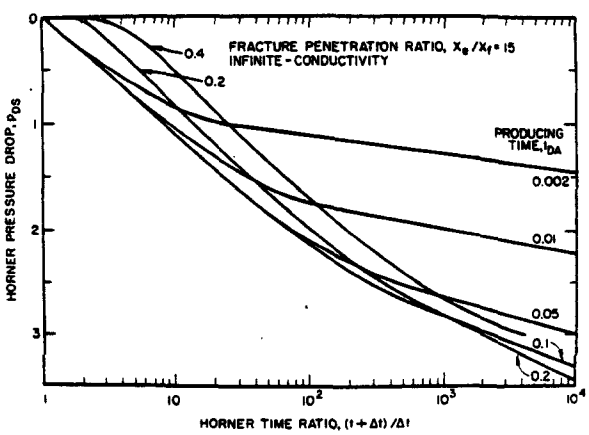


FIG. 10 — HORNER GRAPH FOR VERTICALLY FRACTURED WELL IN THE CENTER OF A CONSTANT-PRESSURE SQUARE.

falloff data may not apply to fractured wells unless producing times are very large.

Conventional well test analysis with a Horner graph to calculate average reservoir pressure required the use of the Matthews-Brons-Hazebroek (MBH)[18] ($p^* - \bar{p}$) functions. The false pressure, $p^*$, was obtained by extrapolating the proper straight line to a time ratio of unity. Determination of MBH functions to calculate $p_i$, and then $\bar{p}$, did not appear worthwhile, however, because of the lack of an identifiable straight line with the proper slope on a Horner graph.

## THE UNIFORM-FLUX FRACTURE

Considering the obvious difficulties involved in the graphical differentiation of the Horner and MDH graphs and associated problems in determining correct slopes, the uniform-flux case was not examined in detail. The type-curve approach was more advantageous in determining the permeability-thickness product and fracture length. However, on a quantitative basis, buildup pressures were different for this case. Thus, graphs similar to Fig. 8 were useful for determining average reservoir pressures. Figs. 11 through 14 present the appropriate graphs for four values of $x_e/x_f$.

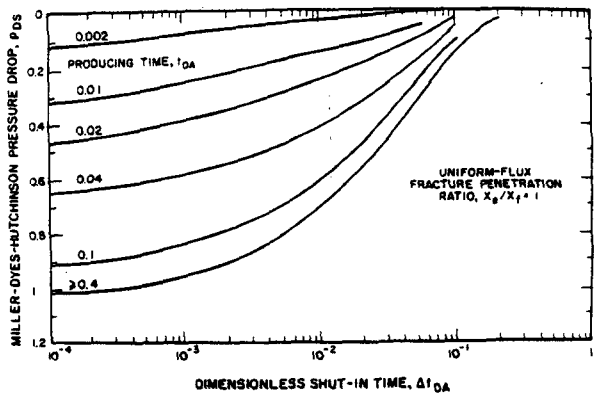


FIG. 11 — MILLER-DYES-HUTCHINSON BUILDUP GRAPH FOR VERTICALLY FRACTURED WELL IN A CONSTANT-PRESSURE SQUARE (UNIFORM-FLUX) ($x_e/x_f = 1$).

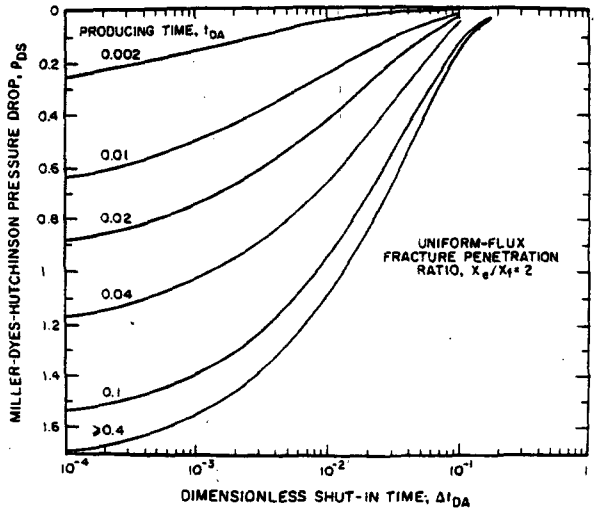


FIG. 12 — MILLER-DYES-HUTCHINSON BUILDUP GRAPH FOR VERTICALLY FRACTURED WELL IN A CONSTANT-PRESSURE SQUARE (UNIFORM-FLUX) ($x_e/x_f = 2$).

## DISCUSSION

The main purpose of this study was to fill a gap in the existing knowledge of fractured well analysis especially the determination of average reservoir pressure. Although many specific quantitative conclusions are presented, the important results are general in nature. For example, the log-log type-curve matching procedure was determined best for finding formation permeability and fracture length, whereas the MDH method appeared to be best for determining average reservoir pressure. In addition, although the Horner method was more reliable than the MDH method for determining the $kh$ product, it did not compare favorably with the log-log approach. The Horner graph was not useful for diagnostic purposes in identifying the constant-pressure outer boundary as in the unfractured well case.

Some unsolved problems regarding fractured wells should be mentioned. Our results, for example, apply only to the injection-production pattern shown in Fig. 15 and this is but one of the many orientations possible. In fact, since sweep efficiency

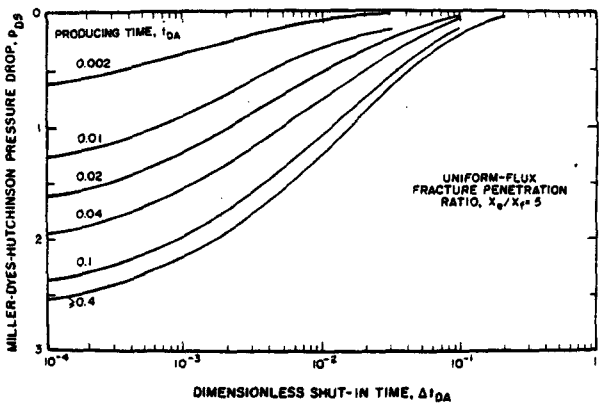


FIG. 13 — MILLER-DYES-HUTCHINSON BUILDUP GRAPH FOR VERTICALLY FRACTURED WELL IN A CONSTANT-PRESSURE SQUARE (UNIFORM-FLUX) ($x_e/x_f = 5$).

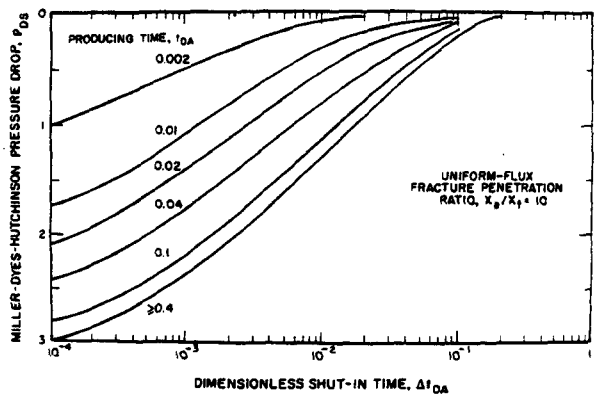


FIG. 14 — MILLER-DYES-HUTCHINSON BUILDUP GRAPH FOR VERTICALLY FRACTURED WELL IN A CONSTANT-PRESSURE SQUARE (UNIFORM-FLUX) ($x_e/x_f = 10$).

considerations are of primary importance, a fracture orientation at a 45° angle to that shown in Fig. 15 would be preferred. If the fracture orientation is different from that considered here, one would expect the drawdown behavior to be close to that shown here for larger fracture penetration ratios. However, for small fracture penetration ratios these results would not apply. Further, it is not evident whether the average reservoir pressure would equal that found by this study even for large penetration ratios. The problems indicate significant areas for further study.

## NOMENCLATURE

$A$ = area, sq ft
$B$ = formation volume factor, RB/STB
$C_A$ = shape factor for a well in the center of a square = 30.88
$c_t$ = system compressibility, $psi^{-1}$
$h$ = thickness of the formation, ft
$k$ = permeability, md
$p$ = fluid pressure, psi
$\bar{p}$ = average pressure in the system, psi
$p_D$ = dimensionless pressure drop
$\bar{p}_D$ = dimensionless average pressure drop
$p_{wD}$ = dimensionless wellbore pressure drop
$p_{wf}$ = flowing well pressure, psi
$p_{ws}$ = shut-in well pressure, psi
$q$ = rate (positive for production and negative for injection), STB/D
$r'_w$ = effective wellbore radius, ft
$t$ = time, hours
$t_{DA}$ = dimensionless time based on drainage area
$\Delta t$ = shut-in time, hours
$x_e; y_e$ = half-length of the reservoir dimensions
$x_f$ = fracture half-length, ft
$\phi$ = porosity
$\mu$ = viscosity of liquid, cp
$\gamma$ = Eulers constant

### SUBSCRIPTS

$D$ = dimensionless
$i$ = initial
$w$ = well
$wf$ = well flowing
$ws$ = well shut-in

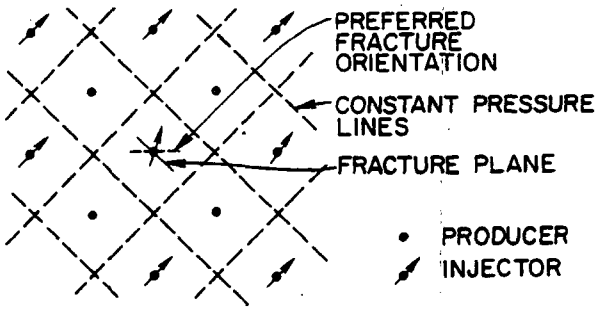


FIG. 15 — REPRESENTATION OF PATTERN ARRANGEMENT WITH FRACTURE PLANE.


## ACKNOWLEDGMENTS

The authors thank the Dept. of Petroleum Engineering of the U. of Tulsa for financial support and The Agency for International Development, Washington, D. C. for financial assistance to Nico Hadinoto.


## REFERENCES


1. Gringarten, A. C., Ramey, H. J., Jr., and Raghavan, R.: "Unsteady-State Pressure Distributions Created by a Well with a Single Infinite-Conductivity Vertical Fracture," *Soc. Pet. Eng. J.* (Aug. 1974) 347-360; *Trans.*, AIME, Vol. 257.
2. Gringarten, A. C., Ramey, H. J., Jr., and Raghavan, R.: "Applied Pressure Analysis for Fractured Wells," *J. Pet. Tech.* (July 1975) 887-892; *Trans.*, AIME, Vol. ~~260.~~ 259
3. Russell, D. G. and Truitt, N. E.: "Transient Pressure Behavior in Vertically Fractured Reservoirs," *J. Pet. Tech.* (Oct. 1964) 1159-1170; *Trans.*, AIME, Vol. 231.
4. Kumar, A. and Ramey, H. J., Jr.: "Well Test Analysis for a Well in a Constant Pressure Square," *Soc. Pet. Eng. J.* (April 1974) 107.
5. Ramey, H. J., Jr., Kumar, A., and Gulati, M. S.: *Gas Well Test Analysis Under Water Drive Conditions*, monograph on Project 61-51, American Gas Assn., Arlington, Va., 312.
6. Ramey, H. J., Jr., and Cobb, W. M.: "A General Pressure Buildup Theory for a Well in a Closed Drainage Area," *J. Pet. Tech.* (Dec. 1971) 1493-1505; *Trans.*, AIME, Vol. 251.
7. Gringarten, A. C. and Ramey, H. J., Jr.: "The Use of Source and Greens Functions in the Solution of Unsteady Flow Problems in Reservoirs," *Soc. Pet. Eng. J.* (Oct. 1973) 285-296; *Trans.*, AIME, Vol. 254.
8. Hurst, W., Haynie, O. K., and Walker, R. N.: "New Concepts Extend Pressure Buildup Analysis," *Pet. Eng.* (Aug. 1962) 65-72.
9. Prats, M.: "Effect of Vertical Fractures on Reservoir Behavior — Incompressible-Fluid Case," *Soc. Pet. Eng. J.* (June 1961) 105-118; *Trans.*, AIME, Vol. 222.
10. Prats, M., Hazebroek, P., and Strickler, W. R.: "Effect of Vertical Fractures on Reservoir Behavior — Compressible-Fluid Case," *Soc. Pet. Eng. J.* (June 1962) 87-94; *Trans.*, AIME, Vol. 225.
11. Muskat, M.: "Use of Data on Buildup of Bottom-Hole Pressures," *Trans.*, AIME, Vol. 123, 44-48.
12. Miller, C. C., Dyes, A. B., and Hutchinson, C. A., Jr.: "The Estimation of Permeability and Reservoir Pressure from Bottom-Hole Pressure Build-Up Characteristics," *Trans.*, AIME, Vol. 189, 91-104.
13. Horner, D. R.: "Pressure Buildup in Wells," *Proc.*, Third World Pet. Cong., E. J. Brill, Leiden, The Netherlands (1951) Vol. 11, 503-521.
14. Clark, K. K.: "Transient Pressure Testing of Fractured Water Injection Wells," *J. Pet. Tech.* (June 1968) 639-643; *Trans.*, AIME, Vol. 231.
15. Agarwal, R. G., Al-Hussainy, R., and Ramey, H. J., Jr.: "An Investigation of Wellbore Storage and Skin Effect in Unsteady Liquid Flow — I. Analytical Treatment," *Soc. Pet. Eng. J.* (Sept. 1970) 279-290; *Trans.*, AIME, Vol. 249.

16. Raghavan, R., Cady, G. V., and Ramey, H. J., Jr.: "Well Test Analysis for Vertically Fractured Wells," *J. Pet. Tech.* (Aug. 1972) 1014-1020; *Trans.*, AIME, Vol. 253.

17. Perrine, R. L.: "Analysis of Pressure Build-Up Curves," *Drill. and Prod. Prac.*, API (1956) 482.

18. Matthews, C. S., Brons, F., and Hazebroek, P.: "A Method for Determination of Average Pressure in a Bounded Reservoir," *Trans.*, AIME, Vol. 201, 182-191.

***